CR-54510

[redacted]

[redacted]

GENERAL DYNAMICS

Convair Division

[redacted]

TRANSONIC BUFFETING OF THE CENTAUR INTERSTAGE ADAPTER

Report No. GDA63-1204

November 19, 1963

under NASA contract NAS 3-3232

MIN

Prepared by

R. R. Mitchell

TABLE OF CONTENTS

TRANSONIC BUFFETING OF THE CENTAUR INTERSTAGE ADAPTER

Foreword

This report contains an analytic solution to the transonic buffeting of a simply supported cylindrical shell. Data from the free vibration tests of the Centaur Interstage Adapter and the results of this analysis are used to determine the adapter's buffet characteristics.

Introduction

This study was initiated to determine the ability of the Centaur Interstage Adapter to withstand transonic buffeting loads. A previous "one mode" analysis of this problem was suspected of being unrealistic and possibly nonconservative based on new fluctuating pressure power spectral densities and past experience with shell-like structures.

The solution to a buffeting problem contains the random vibration analysis of the structure involved and a thorough knowledge of the input pressure power spectral density or correlation function. This problem is further complicated because while the pressure field varies from point to point at any instant, its variation at any given point fluctuates irregularly with time and the wide frequency spectrum results in many shell modes of vibration being excited.

The results of this analysis include the RMS deflections, bending moments, and shear forces in the rings and stringers of the adapter. The solution for these quantities is in series form and due to the relatively slow convergence of the series a digital computer solution was deemed mandatory.

The equations of motion of a cylindrical shell, incorporating the average inertia and stiffness properties of the adapter, are used as a model and the method of normal modes is employed.

Based on experimental frequencies, damping values, and extrapolated input power spectral density data, the RMS values above were computed by hand for the original adapter design and for the adapter with additional and stiffened rings.

Random Vibration Theory

Consider as the basic model a multidegree of freedom system subjected to a one dimensional disturbance. The response of such a system can be represented by

$$\alpha(x,y,z,t) = \sum_i \sum_j \alpha_{ij}(x,y,z)\, q_{ij}(t) \tag{1.1}$$

where $\alpha(x, y, z, t)$ are quantities that represent any particular item of interest such as stress, deflection, bending moment etc., at a point (x, y, z) in the structure: $\alpha_{ij}(x, y, z)$ are quantities that represent any particular item of interest at a point (x, y, z) in the structure due to a unit displacement in the ij^{th} normal mode; $q_{ij}(t)$ are the generalized coordinates associated with the normal modes $\phi_{ij}(x, y, z)$.

The generalized coordinates can be approximated by repeated solutions of

$$\ddot{q}_{ij} + 2\xi_{ij}\omega_{ij}\dot{q}_{ij} + \omega_{ij}^2 q_{ij} = Q_{ij}(t)/M_{ij} \tag{1.2}$$

where $Q_{ij}(t)$ is the generalized force, M_{ij} the generalized mass, ω_{ij} the ij^{th} principal frequency, and ξ_{ij} the modal damping. Specifically,

$$Q_{ij}(t) = \int_v F(x,y,z,t)\,\phi_{ij}(x,y,z)\,dv \tag{1.3}$$

$$M_{ij} = \int_v \rho(x,y,z)\,\phi_{ij}^2(x,y,z)\,dv$$

Assume that the forcing function is separable with respect to space and time, i.e.,

$$F(x,y,z,t) = F(x,y,z)\, f(t) \tag{1.4}$$

Substituting Equation (1.4) into (1.3)

$$Q_{ij}(t) = f(t)\int_v P(x,y,z)\,\phi_{ij}(x,y,z)\,dv \equiv f(t)\,P_{ij} \tag{1.5}$$

The solution of Equation (1.2) is

$$q_{ij}(t) = \int_0^\infty h_{ij}(\tau) f(t-\tau)\,d\tau = \frac{1}{2\pi}\int_{-\infty}^{\infty} H_{ij}(i\omega) f(\omega)\, e^{i\omega t}\,d\omega \tag{1.6}$$

where

$$h_{ij}(\tau) = \frac{P_{ij}}{M_{ij}\,\omega_{ij}\sqrt{1-\xi_{ij}^2}}\, e^{-\omega_{ij}\xi_{ij}\tau} \sin\sqrt{1-\xi_{ij}^2}\;\omega_{ij}\,\tau \tag{1.7}$$

and $$H_{ij}(i\omega) = \int_{-\infty}^{\infty} h_{ij}(\tau)\, e^{-i\omega t}\,d\tau$$

$$= \frac{P_{ij}}{M_{ij}} \frac{1}{(\omega_{ij}^2-\omega^2)+(2i\,\xi_{ij}\,\omega\,\omega_{ij})} \tag{1.8}$$

Hence the response of the system is characterized either by its complex frequency response or its unit impulse response. Equation (1.1) becomes

$$\alpha(x,y,z,t) = \sum_i \sum_j \alpha_{ij}(x,y,z)\int_0^\infty h_{ij}(\tau) f(t-\tau)\,d\tau \tag{1.9}$$

or alternatively

$$\alpha(x,y,z,t) = \sum_i \sum_j \alpha_{ij}(x,y,z) \frac{1}{2\pi} \int_{-\infty}^{\infty} H_{ij}(i\omega) f(\omega) e^{i\omega t} d\omega \quad (1.10)$$

Now consider f(t) to be a sampled function from a stationary random process, i.e., a random process for which the ensemble avera es over all possible records of the process are independent of the time at which these averages are taken for each record. Important statistical properties of the excitation random process are the mean

$$\bar{f} = \underset{T\to\infty}{\text{LIM}} \frac{1}{2T} \int_{-T}^{T} f(t)\,dt \equiv \left\langle \left\{ f(t) \right\} \right\rangle_{AV} \quad (1.11)$$

the mean square or average power

$$\bar{f}^2 + \overline{f}^2 = \left\langle \left\{ f^2(t) \right\} \right\rangle_{AV} \quad (1.12)$$

the autocorrelation function

$$R_f(\tau) = \left\langle \left\{ f(t) f(t+\tau) \right\} \right\rangle \quad (1.13)$$

and the power spectral density.

$$\Phi_f(\omega) = 2\int_{-\infty}^{\infty} R_f(\tau) e^{-i\omega t} d\tau \quad (1.14)$$

Conversely, the Fourier transform of Equation (1.14) is

$$R_f(\tau) = \frac{1}{4\pi} \int_{-\infty}^{\infty} \Phi_f(\omega) e^{i\omega t} d\omega \quad (1.15)$$

Note that the mean square of the input random function is given by

$$R_f(0) = \bar{f}^2 + \overline{f}^2 = \frac{1}{4\pi} \int_{-\infty}^{\infty} \Phi_f(\omega)\, d\omega \quad (1.16)$$

The properties of the response $\alpha(x,y,z,t)$ can now be determined. The assumption is made for this analysis that the mean of the excitation, $\bar{f}$, is zero which implies that the mean of the response, $\bar{\alpha}$, is also zero.

The autocorrelation function of the response, $R_\alpha(\tau)$, is by definition

$$R_\alpha(\tau) = \lim_{T\to\infty} \frac{1}{2T}\int_{-T}^{T} \alpha(x,y,z,t)\alpha(x,y,z,t+\tau)\,dt \equiv \left\langle \alpha(x,y,z,t)\,\alpha(x,y,z,t+\tau) \right\rangle_{AV} \tag{1.17}$$

Substituting Equation (1.9) twice in Equation (1.17) and interchanging the order of integration

$$R_\alpha(\tau) = \sum_i \sum_j \sum_K \sum_l \alpha_{ij}(x,y,z)\alpha_{Kl}(x,y,z) \int_0^\infty h_{Kl}(\tau_1)\,d\tau_1 \int_0^\infty h_{ij}(\tau_2) R_f(\tau+\tau_2-\tau_1)\,d\tau_2 \tag{1.18}$$

which represents a double convolution of the excitation autocorrelation function.

The power spectral density of the response, $\Phi(\omega)$, is by definition

$$\Phi_\alpha(\omega) = 2\int_{-\infty}^{\infty} R_\alpha(\tau) e^{-i\omega t}\,d\tau$$

which eventually yields, after substitution of Equation (1.18),

$$\Phi_\alpha(\omega) = \sum_i \sum_j \sum_K \sum_l \alpha_{ij}(x,y,z)\alpha_{Kl}(x,y,z) H_{ij}(i\omega) H_{Kl}^{*}(i\omega) \Phi_f(\omega) \tag{1.19}$$

Since $\Phi_\alpha(\omega)$ must be a real quantity, the real part of $H_{ij} H^*_{kl}$ is taken and Equation (1.19) becomes

$$\Phi_\alpha(\omega) = \sum_i \sum_j \sum_K \sum_\ell \alpha_{ij}(x,y,z)\,\alpha_{K\ell}(x,y,z)\,K_{ijK\ell}(\omega)\,\Phi_f(\omega) \tag{1.20}$$

where

$$K_{ijK\ell}(\omega) = \frac{P_{ij}\,P_{K\ell}}{M_{ij}\,M_{K\ell}} \left\{ \frac{(\omega_{ij}^2-\omega^2)(\omega_{K\ell}^2-\omega^2)+(2\xi_{ij}\,\omega\omega_{ij})(2\xi_{K\ell}\,\omega\omega_{K\ell})}{\left[(\omega_{ij}^2-\omega^2)^2+(2\xi_{ij}\,\omega\omega_{ij})^2\right]\left[(\omega_{K\ell}^2-\omega^2)^2+(2\xi_{K\ell}\,\omega\omega_{K\ell})^2\right]} \right\} \tag{1.21}$$

The mean square of the response is the zero time autocorrelation of the response which can be evaluated from Equation (1.20) and the Fourier transform in Equation (1.15).

$$\overline{\alpha^2} = R_\alpha(0) = \frac{1}{4\pi} \sum_i \sum_j \sum_K \sum_\ell \alpha_{ij}(x,y,z)\,\alpha_{K\ell}(x,y,z) \int_{-\infty}^{\infty} K_{ijK\ell}(\omega)\,\Phi_f(\omega)\,d\omega \tag{1.22}$$

If the input power spectral density is assumed to be white noise, i.e., $\Phi_f(\omega) = \Phi_o$ then a contour integration of $K_{ijK\ell}(\omega)$ results in Equation (1.23).

$$\overline{\alpha^2} = \frac{1}{2\pi} \sum_i \sum_j \sum_K \sum_\ell \alpha_{ij}(x,y,z)\,\alpha_{K\ell}(x,y,z)\,\Phi_o\,D_{ijK\ell} \tag{1.23}$$

where

$$D_{ijK\ell} = \frac{2\pi P_{ij}\,P_{K\ell}}{\omega_{ij}^3\,M_{ij}\,M_{K\ell}} \left\{ \frac{\left(\frac{\omega_{K\ell}}{\omega_{ij}}\right)\xi_{K\ell}+\xi_{ij}}{\left(\frac{\omega_{K\ell}}{\omega_{ij}}\right)^4+4\left(\frac{\omega_{K\ell}}{\omega_{ij}}\right)^3\xi_{ij}\,\xi_{K\ell}+2\left(\frac{\omega_{K\ell}}{\omega_{ij}}\right)^2\left(2\xi_{ij}^2+2\xi_{K\ell}^2-1\right)+4\left(\frac{\omega_{K\ell}}{\omega_{ij}}\right)\xi_{ij}\,\xi_{K\ell}+1} \right\} \tag{1.24}$$

Assuming equal damping, ξ , for all modes reduces Equation (1.24) to

$$D_{ijkl} = \frac{2\pi P_{ij} P_{kl}}{\omega_{ij}^3 M_{ij} M_{kl}} \left\{ \frac{\left[\left(\frac{\omega_{kl}}{\omega_{ij}}\right) + 1\right]\xi}{\left[\left(\frac{\omega_{kl}}{\omega_{ij}}\right)^2 - 1\right]^2 + 4\xi^2 \left(\frac{\omega_{kl}}{\omega_{ij}}\right)\left[\left(\frac{\omega_{kl}}{\omega_{ij}}\right) + 1\right]^2} \right\} \qquad (1.25)$$

Equation (1.23) can be written conveniently

$$\overline{\alpha^2} = \Phi_o \sum_i \sum_j \alpha_{ij}^2(x,y,z) \frac{P_{ij}^2}{M_{ij}^2} \frac{1}{\omega_{ij}^3} \frac{1}{8\xi} \qquad (1.26)$$

$$+ \frac{\Phi_o}{2\pi} \sum_i \sum_j \sum_k \sum_l \alpha_{ij}(x,y,z)\, \alpha_{kl}(x,y,z)\, D_{ijkl}$$

$$i \neq k$$
$$j \neq l$$

The first term of Equation (1.26) is assumed to be the major contributor to the mean square of $\alpha(x,y,z,t)$ and the effect of the second term, which is neglected in the hand calculations, is investigated in the digital computer solution.

Free and Forced Vibrations of the Cylindrical Shell Model

For the purpose of the computer analysis the adapter will be represented as a cylindrical shell with inertial properties that match those of the adapter and with stiffness properities that results in an experimentally determined 50 cps lowest natural frequency.

The equations of motion of a circular cylindrical shell are

$$\frac{\partial u^2}{\partial x^2} + \frac{1-\nu}{2}\frac{\partial u^2}{\partial s^2} + \frac{1+\nu}{2}\frac{\partial^2 v}{\partial x \partial s} + \frac{\nu}{a}\frac{\partial w}{\partial x} - \left(\frac{\rho}{E^*}\right)\frac{\partial^2 u}{\partial t^2} = 0$$

$$\frac{1+\nu}{2}\frac{\partial^2 u}{\partial x \partial s} + \frac{1-\nu}{2}(1+4\alpha)\frac{\partial^2 v}{\partial x^2} + (1+\alpha)\frac{\partial^2 v}{\partial s^2} + \frac{1}{a}\frac{\partial w}{\partial s} - a\alpha(2-\nu)\frac{\partial^3 w}{\partial x^2 \partial s} \qquad (2.1)$$

$$-a\alpha\frac{\partial^3 w}{\partial s^3} - \left(\frac{\rho}{E^*}\right)\frac{\partial^2 v}{\partial t^2} = 0$$

$$\frac{\nu}{a}\frac{\partial u}{\partial x} + \left[\frac{1}{a} - a\alpha\frac{\partial^2}{\partial s^2} - a\alpha(2-\nu)\frac{\partial^2}{\partial x^2}\right]\frac{\partial v}{\partial s} + a^2\alpha\nabla^4 w + \frac{w}{a^2} + \left(\frac{\rho}{E^*}\right)\frac{\partial^2 w}{\partial t^2} = 0$$

The solutions for the three displacements (u, v, w) in Equation (2.1) can be expanded in terms of normal modes.

$$u = \sum_i \sum_j \alpha_{ij}(x,s)\, q_{ij}(t)$$

$$v = \sum_i \sum_j \beta_{ij}(x,s)\, q_{ij}(t) \qquad (2.2)$$

$$w = \sum_i \sum_j \gamma_{ij}(x,s)\, q_{ij}(t)$$

where for simply supported boundary conditions the normal modes can be expressed as

$$\alpha_{ij}(x,s) = A_{ij} \cos \frac{i\pi}{L} x \cos \frac{j}{a} s \qquad (2.3)$$

$$B_{ij}(x,s) = B_{ij} \sin \frac{i\pi}{L} x \sin \frac{j}{a} s$$

$$\gamma_{ij}(x,s) = C_{ij} \sin \frac{i\pi}{L} x \cos \frac{j}{a} s$$

Substitution of equations (2.2) and (2.3) into (2.1) results in frequency equation (see Reference 2 for details).

$$\begin{vmatrix} a_{11}-r^2 & a_{12} & a_{13} \\ a_{21} & a_{22}-r^2 & a_{23} \\ a_{31} & a_{32} & a_{33}-r^2 \end{vmatrix} = 0 \qquad (2.4)$$

The amplitude ratios $\frac{A_{ij}}{C_{ij}}$ and $\frac{B_{ij}}{C_{ij}}$ are obtained from equations (2.5).

$$(a_{11}-r_{ij}^2)A_{ij} + a_{12}B_{ij} + a_{13}C_{ij} = 0 \qquad (2.5)$$

$$a_{21}A_{ij} + (a_{22}-r_{ij}^2)B_{ij} + a_{23}C_{ij} = 0$$

$$a_{31}A_{ij} + a_{32}B_{ij} + (a_{33}-r_{ij}^2)C_{ij} = 0$$

Through the use of the [illegible] condition, equation (2.5), the [illegible] ratios from equation (2.5), the [illegible] coefficients A_{ij}, B_{ij}, and C_{ij} were determined explicitly.

$$\int_0^L \int_0^{2\pi a} \left[\alpha_{ij}^2 + \beta_{ij}^2 + \gamma_{ij}^2\right] ds\, dx = \frac{\pi a L}{2} \tag{2.6}$$

Substituting Equation (2.3) into (2.6) the normalizing condition becomes:

$$A_{ij}^2 + B_{ij}^2 + C_{ij}^2 = 1 \tag{2.7}$$

The generalized mass is written as

$$M_{ij} = \rho h \int_0^L \int_0^{2\pi a} \left[\alpha_{ij}^2 + \beta_{ij}^2 + \gamma_{ij}^2\right] ds\, dx \tag{2.8}$$

Substituting Equation (2.3) into (2.8) the generalized mass becomes:

$$M_{ij} = \rho h \frac{\pi a L}{2} \tag{2.9}$$

The calculation of the generalized force requires a knowledge of the spatial force distribution, P(x,s), in Equation (1.4). Two different spatial force distributions are employed here. The first force distribution matches the mode; i.e, the force is proportional to and in the opposite direction of the displacement.

$$P(x,s) = \sin \frac{i\pi}{L} x \cos \frac{j}{a} s \tag{2.10}$$

From Equation (1.5) the generalized force is written as

$$Q_{ij} = f(t) \int_0^L \int_0^{2\pi a} P(x,s)\, \gamma_{ij}(x,s)\, ds\, dx \tag{2.11}$$

which becomes after substitution of Equations (2.10) and (2.3)

$$Q_{ij} = f(t) \frac{\pi a L}{2} C_{ij} \tag{2.12}$$

The other force distribution is used in the hand computations and more exactly reflects the effects of the hydrogen boost pump fairing, insulation panels, retrorocket fairings, and the destruct package. (See Figures II and III).

$$P(x,s) = P_1(x,s) + P_2(x,s) \tag{2.13}$$

The force distribution $P_1(x,s)$ represents the effects of the insulation panels and the hydrogen boost pump fairing and $P_2(x,s)$ takes into account the five retrorocket fairings and the destruct package. The two force distributions overlap somewhat but this adds a bit of conservatism and greatly simplifies the analysis.

$$P_1(x,s)=\begin{cases} A \sin\frac{i\pi}{L} x \cos\frac{j}{a} s & ; 0\le x\le dL, -\Delta S\le s\le \Delta S \\ A \sin\frac{i\pi}{L} x \cos\frac{j}{a} s \left[1+e \sin\left(\frac{\frac{x}{L}-d}{1-d}\frac{\pi}{2}\right)\right] & ; dL< x\le L, -\Delta S\le s\le \Delta S \\ \sin\frac{i\pi}{L} x \cos\frac{j}{a} s \left[1+c \sin\frac{\pi}{bL} x\right] & ; 0\le x\le bL,\ \Delta S< s< 2\pi a-\Delta S \\ \sin\frac{i\pi}{L} x \cos\frac{j}{a} s & ; bL< x\le L,\ \Delta S< s< 2\pi a-\Delta S \end{cases} \quad (2.14)$$

$P_1(x,s)$ is represented graphically in Figure III. The circumferential force distribution is uniform over both the insulation panels and the hydrogen boost pump fairing but of magnitude A in the region of the hydrogen boost pump fairing. For clarity the sinusoidal terms resulting from the mode shape which are included in Equation (2.14) are not shown in Figure III. The axial force distributions, which are derived from Figure II, and their approximations (Equation 2.14) are plotted as a function of the adapter length.

$$P_2(x,s)=\sum_{K=1}^{6} D_K \sin\frac{i\pi}{L} x \cos\frac{j}{a} s;\ 0\le x\le L, s_K\le s\le s_K+\Delta s_K \quad (2.15)$$

Substitution of Equations (2.13) and (2.3) into (2.11) yields the generalized force

$$Q_{ij}=f(t)C_{ij}\frac{\pi aL}{2}\left\{A\left[\frac{\Delta s}{\pi a}+\frac{\sin\frac{2j}{a}\Delta s}{2\pi j}\right]\left[1+\frac{2e(1-d)}{\pi}\left\{1-\frac{\cos 2i\pi d}{1-16i^2(1-d)^2}\right\}\right]\right. \quad (2.16)$$

$$+\left[1-\frac{\Delta s}{\pi a}-\frac{\sin\frac{2j}{a}\Delta s}{2\pi j}\right]\left[1+\frac{2cb}{\pi}\left\{1-\frac{(1+\cos 2i\pi b)}{2(1-4i^2b^2)}\right\}\right]$$

$$\left.+\sum_{K=1}^{6} D_K\left[\frac{\Delta s_K}{\pi a}+\frac{\cos\frac{2j}{a}s_K \sin\frac{2j}{a}\Delta s_K}{2\pi j}\right]\right\}$$

DISCUSSION

Basic Assumptions & Data

A summary of the assumptions made thus far and necessary additional ones are listed below. The basic data for the different interstage adapter configurations is given in Table I.

1) The mass of the adapter is uniformly distributed.
2) The spatial force distribution for the digital computer program is assumed to match the mode.
3) The input fluctuating pressure power spectral density distributions have a "white noise" frequency distribution and spatial distributions shown in Figure 3.
4) Amplitude ratios to be used in all equations are determined by the cylindrical shell program.
5) RMS results are obtained at the antinodes for the experimental data using the modes $m = 1$, $n = 2 - 7$, and $m = 3$, $n = 3 - 6$
6) The hydrogen boost pump fairing is assumed to be four feet wide and of rectangular cross section.

The results of this study consists of two parts. The first part is a hand calculation of various RMS values based upon experimental vibration characteristics (590 lb. adapter), calculated vibration data (1539 lb. adapter, cf. Reference 5, extrapolated wind tunnel data (cf. Reference 4), and other vibration constants determined by digital computation. As is indicated, two different adapter configurations are used. The 590 lb. configuration consists of the ring - stringer - skin structure only, whereas the 1539 lb. "beefed-up" configuration includes approximately 422 lb. of non-structural weight. The effects of including non-structural weight to the 590 lb. adapter is discussed. The second part of the study uses a cylindrical shell structural model, whose stiffness and inertial properties are equivalent to the average properties of the adapter, to compute natural frequencies and amplitude ratios. A digital computer program then evaluates Equation 1.26 (the cross terms in the quadruple summation were previously neglected) for the needed statistical quantities. For part two, the insulation panel step is the only protuberance considered.

The statistical quantities evaluated are the RMS values of the radial deflection at the antinodes, the bending moment in the rings and stringers, and the shear force in the rings.

The mean square radial deflection, $\overline{w^2}$, is obtained from Equation 1.26 by substituting the radial normal mode shape $\delta_{ij}(x,s)$ for $\alpha_{ij}(x,s)$

$$\overline{W^2} = \frac{\Phi_o}{(\rho h)^2} \sum\sum\sum\sum C_{ij} C_{k\ell} \gamma_{ij} \gamma_{k\ell} \frac{1}{\omega_{ij}^3} \left\{ \frac{\zeta \left(\frac{\omega_{k\ell}}{\omega_{ij}} + 1 \right)}{\left[\left(\frac{\omega_{k\ell}}{\omega_{ij}} \right)^2 - 1 \right]^2 + \zeta^2 \frac{\omega_{k\ell}}{\omega_{ij}} \left[\frac{\omega_{k\ell}}{\omega_{ij}} + 1 \right]^2} \right\} \qquad (3.1)$$

where

$$\gamma_{ij} = C_{ij} \sin \frac{i\pi}{L} x \cos \frac{j}{a} s$$

The rings and stringers are treated as beams and the corresponding beam equations for bending moments and shear are applied.

$$M_x = -EI_x \frac{\partial^2 w}{\partial x^2}$$

$$M_s = -EI_s \frac{\partial^2 w}{\partial s^2} \qquad (3.2)$$

$$Q_s = -EI_s \frac{\partial^3 w}{\partial s^3}$$

Since these quantities are linear functions of the deflection, the mean square values can be evaluated directly.

$$\overline{M_x^2} = \frac{\Phi_o}{(\rho h)^2} (EI_x)^2 \sum_i \sum_j \sum_k \sum_\ell C_{ij} C_{k\ell} \left(\frac{i\pi}{L} \right)^2 \left(\frac{k\pi}{L} \right)^2 \gamma_{ij} \gamma_{k\ell} \frac{1}{\omega_{ij}^3} \left\{ \text{same as Eq. (3.1)} \right\}$$

$$\overline{M_s^2} = \frac{\Phi_o}{(\rho h)^2} (EI_s)^2 \sum_i \sum_j \sum_k \sum_\ell C_{ij} C_{k\ell} \left(\frac{j}{a} \right)^2 \left(\frac{\ell}{a} \right)^2 \gamma_{ij} \gamma_{k\ell} \frac{1}{\omega_{ij}^3} \left\{ \text{same as Eq. (3.1)} \right\} \qquad (3.3)$$

$$\overline{Q_s^2} = \frac{\Phi_o}{(\rho h)^2} (EI_s)^2 \sum_i \sum_j \sum_k \sum_\ell C_{ij} C_{k\ell} \left(\frac{j}{a} \right)^3 \left(\frac{\ell}{a} \right)^3 \gamma_{ij} \gamma_{k\ell} \frac{1}{\omega_{ij}^3} \left\{ \text{same as Eq. (3.1)} \right\}$$

For the hand calculations the cross terms in Equations (3.1) and (3.3) are neglected; i.e, those terms for which i = k and j = l. This results in (cf. Equation 1.26)

$$\overline{W^2} = \frac{\Phi_o}{(\rho h)^2} \sum_{i=1}^{\infty} \sum_{j=0}^{\infty} \frac{P_{ij}^2}{M_{ij}^2} \gamma_{ij}^2 \frac{1}{\omega_{ij}^3} \frac{1}{8\xi}$$

$$\overline{M_x^2} = \frac{\Phi_o}{(\rho h)^2} (EI_x)^2 \sum_{i=1}^{\infty} \sum_{j=0}^{\infty} \frac{P_{ij}^2}{M_{ij}^2} \left(\frac{i\pi}{L}\right)^4 \gamma_{ij}^2 \frac{1}{\omega_{ij}^3} \frac{1}{8\xi} \qquad (3.4)$$

$$\overline{M_s^2} = \frac{\Phi_o}{(\rho h)^2} (EI_s)^2 \sum_{i=1}^{\infty} \sum_{j=0}^{\infty} \frac{P_{ij}^2}{M_{ij}^2} \left(\frac{j}{a}\right)^4 \gamma_{ij}^2 \frac{1}{\omega_{ij}^3} \frac{1}{8\xi}$$

$$\overline{Q_s^2} = \frac{\Phi_o}{(\rho h)^2} (EI_s)^2 \sum_{i=1}^{\infty} \sum_{j=0}^{\infty} \frac{P_{ij}^2}{M_{ij}^2} \left(\frac{j}{a}\right)^6 \gamma_{ij}^2 \frac{1}{\omega_{ij}^3} \frac{1}{8\xi}$$

The results of the hand calculations are given in Table III. The uniform addition of nonstructural weight reduces all RMS values (cf 2nd and 5th columns of Table III) by a factor of $[W_f / W_i]^{-1/4}$ where in this case W_i = 590 lb. and W_f = 590 + 422 = 1012 lb.

A sample calculation of one of the quantities above is of interest to illustrate the convergence characteristics of the double series and to indicate the relative magnitudes of the contribution of the individual modes to the total mean square.

Denoting the term under the double summation sign of $\overline{M_s^2}$ as H_{ij}, i.e

$$H_{ij} = \frac{P_{ij}^2}{M_{ij}^2} \left(\frac{j}{a}\right)^4 \gamma_{ij}^2 \frac{1}{\omega_{ij}^3} \frac{1}{8\xi} \qquad (3.5)$$

the modal values of Hij are evaluated and listed in Table IV for both adapter configurations. It is evident that no single mode completely dominates the contribution to the mean square bending moment and that the mode of lowest natural frequency (m = 1, n = 3) is not the maximum contributor. Therefore, an approximate method based on a one mode analysis is somewhat difficult since it is not immediately clear what mode to use.*

The Hij values converge for m = 1 and increasing circumferential mode numbers (n = 2 - 7) but do not converge for m = 3 and increasing circumferential mode numbers. Any nonconservatism introduced by neglecting the contribution from the m = 3, n = 7, 8, 9 - - - modes, data for which is unavailable, is compensated for by the conservative assumption of a four foot wide rectangular cross section hydrogen boost pump fairing.

---

* An approximation of this type to determine ring bending moments has been suggested. The procedure outlined above for computing the Hij's can be used to determine the maximum contributing mode. Experience with the Centaur Adapter has shown that this mode contributes approximately 50% to 55 % of the RMS ring bending moment and since the input power spectral density data is not well known, a more conservative spatial force distribution can be used to compensate for the neglected contribution from the remaining modes. A "unity correlation" force distribution, i.e., a constant force amplitude opposed to the deflection, results in an increase in RMS values by a factor of $(4/\pi)^2 = 1.62$. Combining the conservative force distribution with the bending moment of the maximum contributing mode yields a result 80% to 90% of the RMS ring bending moment.

The results of the digital computer portion of the solution are dependent upon the natural frequency distribution of the cylindrical shell model. Table II lists the natural frequency distribution and several interesting characteristics are apparent. The frequencies always increase with increasing axial mode number but decrease, reach a minimum, and increase with increasing circumferential mode number. This is the major reason for the slow convergence of the series solution. Also this effect results in many modes of nearly equal frequency which can cause a type of "resonance". A case in point: the natural frequencies of the m = 7, n = 7 and m = 9, n = 10 modes differ by only 0.2% and these are the modal combinations which cause the negative 1% contribution (cf. Table III) to the mean square bending moment in the rings. A similar result occurs for the 1539 lb. adapter.

Table III shows the results of the digital computation and the RMS bending moments are considerably larger than the hand calculated results. The reason for this is twofold: first the natural frequency distribution of the cylindrical shell model is a poor approximation to that of the Centaur Adapter, i.e., in general the frequencies are much higher (the lowest natural frequencies are the same) and second all combinations of 400 modes or 160,000 terms were used in the digital computation whereas only 10 terms were used in the hand calculations. The percentage values shown in Table III represent the contribution of the second term in Equation 1.26 to the total mean square. These cross terms are obviously not small for the bending moment in the stringers but could be neglected in the other cases. Historically the cross terms have always been small and the reason for this unusual result is not immediately obvious.

A convenient parameter to use for convergence analyses is the space average of the mean square response or the average mean square response. This is obtained by integrating the response function over the total area of the structure and in doing so becoming independent of any spatial coordinates. This facilitates the convergence analysis but restricts the scope of the results since no precise information can be obtained about the convergence of the response at a point. It is interesting to note at this point that if Equation 1.26 is integrated over the area of the cylinder, the second term is zero because of the orthogonality condition. This means that the average mean square response is independent of the cross terms although the response at a point is not. All responses computed converged with respect to both axial and circumferential mode number except the stringer bending moment response. This response, $\overline{M_x^2}$, converged with respect to the circumferential mode number but after twenty axial modes no definite indication of convergence occurred. The corresponding computer results in Table III should be read with this in mind.

Conclusions

The RMS and 3σ transonic buffeting characteristics of the redesigned Centaur Interstage Adapter are

	RMS	3σ
w (in.)	0.105	0.315
M_x (in. lb)	40.4	121.2
M_s (in. lb)	2620.0	7800.0
Q_s (lb.)	203.0	609.0

The cylindrical shell approximation to the Centaur Interstage Adapter is not satisfactory since the frequency distributions differ so widely and it is suggested for future investigations that an orthotropic shell approach be taken to better approximate ring-stringer-skin structures.

Other suggested investigations include a method of improving the convergence of the response, determining what conditions result in non-negligible cross terms in Equation 1.26, and continued experimental study of fluctuating pressure power spectral density characteristics. It is possible that the cross power spectral density characteristics are not negligible and should be included in a refined analysis. Also, if band limited white noise satisfactorily approximates the actual input power spectral density, the convergence of the response can be radically improved.

The approximate analysis, described in the footnote on page 15 of the discussion, can be used for pre-design studies of interstage adapters of the Centaur type but due caution should be employed in any general application.

Prepared by R. R. Mitchell
R. R. Mitchell (x2183)

Checked by R. Schuett
R. Schuett (x4674)
Design Specialist

Approved by L. L. Fontenot
L. L. Fontenot (x3295)
Design Specialist

cc: A. Leondis
J. Conly
J. Martin
E. Noble
J. Stanley
M. Wohltmann
C. Enzmann
J. Kittle
A. Zoldos

FIGURE I

590 LB. AND 1539 LB. ADAPTER CONFIGURATIONS

The skin of both adapters is 0.032 2024T4 aluminum.

There are 45 stringers spaced approximately 8 - $\frac{1}{2}$ inches on center around the circumference.

The 590 lb configuration has 11 Z Frames spaced approximately 14.6 inches on center longitudinally.

The 1539 lb. configuration has 21 H Frames spaced approximately 7.3 inches on center longitudinally and 422 lb. of non structural weight.

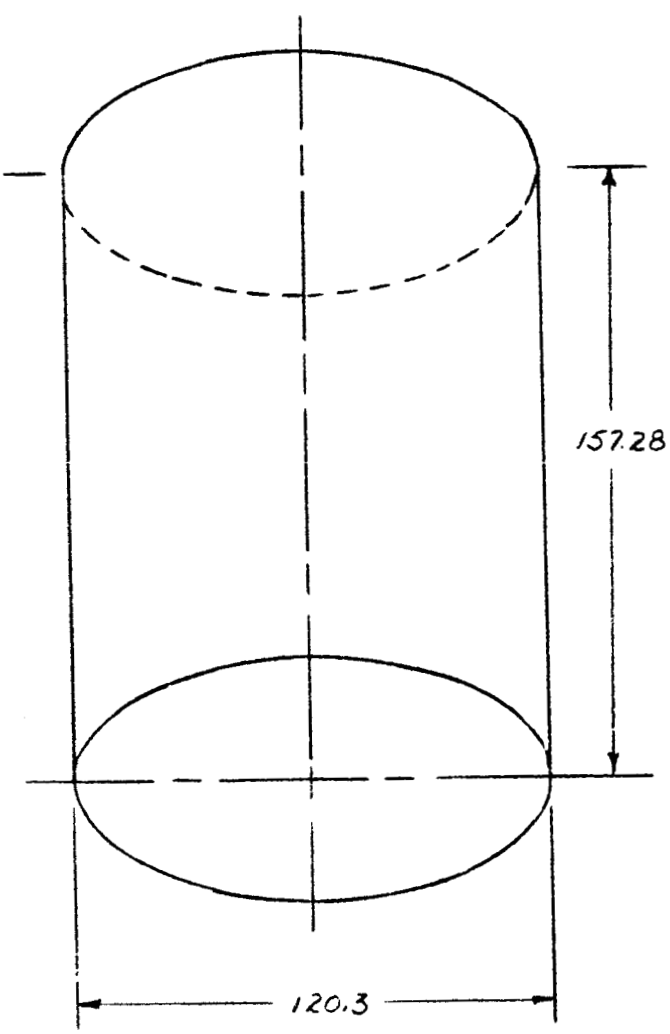

Stringer Detail

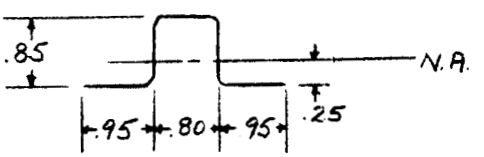

Material: 0.050 7075T6 aluminum
Area moment of inertia = .0278 in^4

Z-Frame Detail

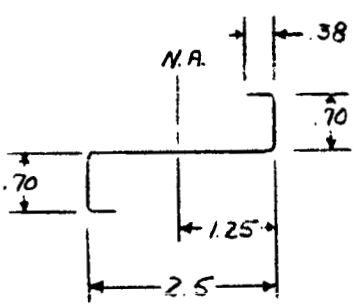

Material: 0.040 7075T6 Aluminum
Area moment of inertia = .1454 in^4

H Frame Detail

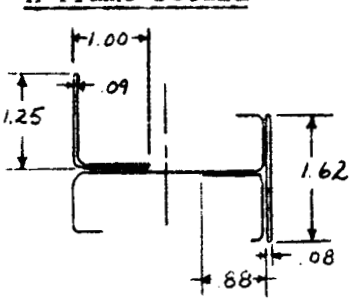

Material: 0.040 7075T6(unless otherwise specified)
Area moment of inertia = 0.657 in^4
Other dimensions are the same as Z-Frame above.

FIGURE II

SPATIAL POWER SPECTRAL DENSITY DISTRIBUTIONS FOR PROTUBERANCES FORWARD OF THE INTERSTAGE ADAPTER

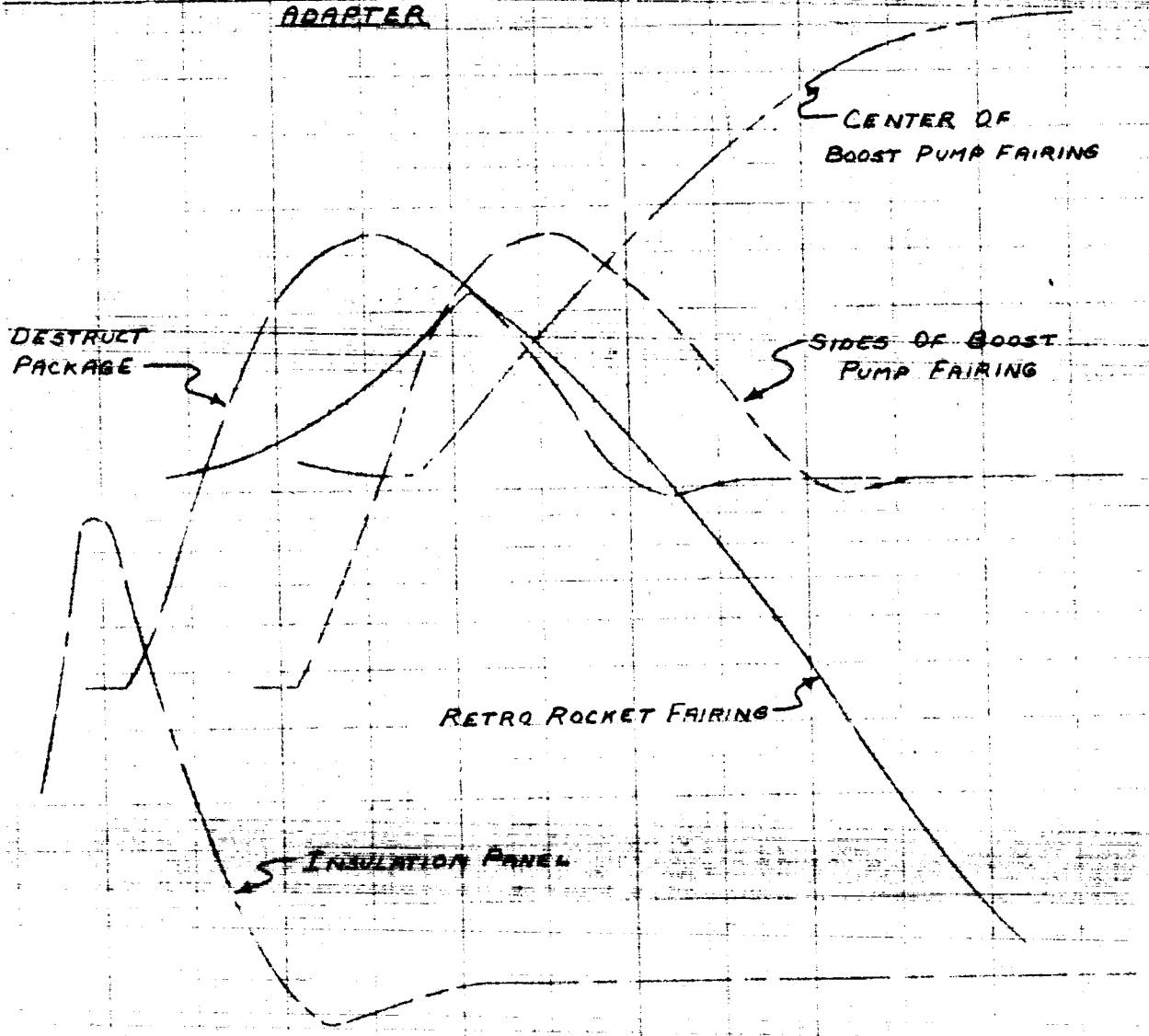

MSG 9-12-4

FIGURE III

Axial and Circumferential Force Distributions

Circumferential Force Distribution

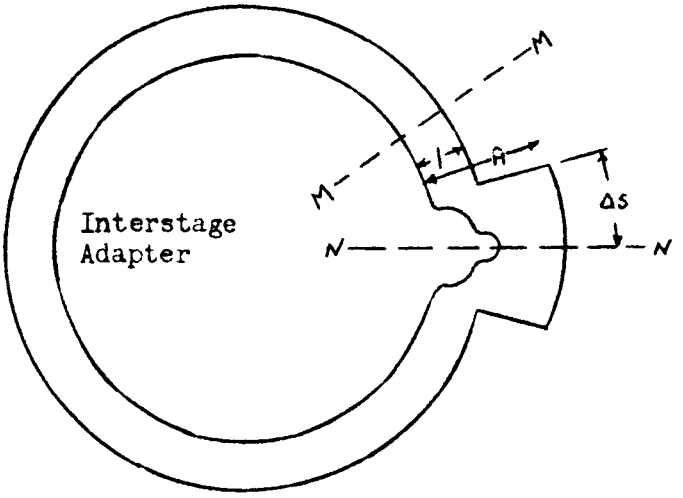

M - M
Insulation
Panel
Axial
Force
Distribution

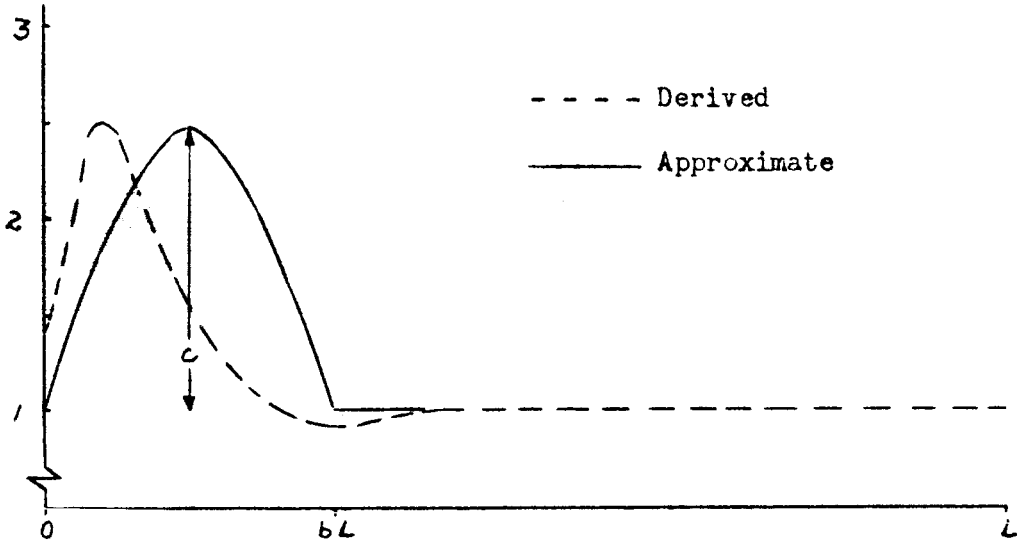

N - N
Hydrogen
Boost pump
Fairing
Axial
Force
Distribution

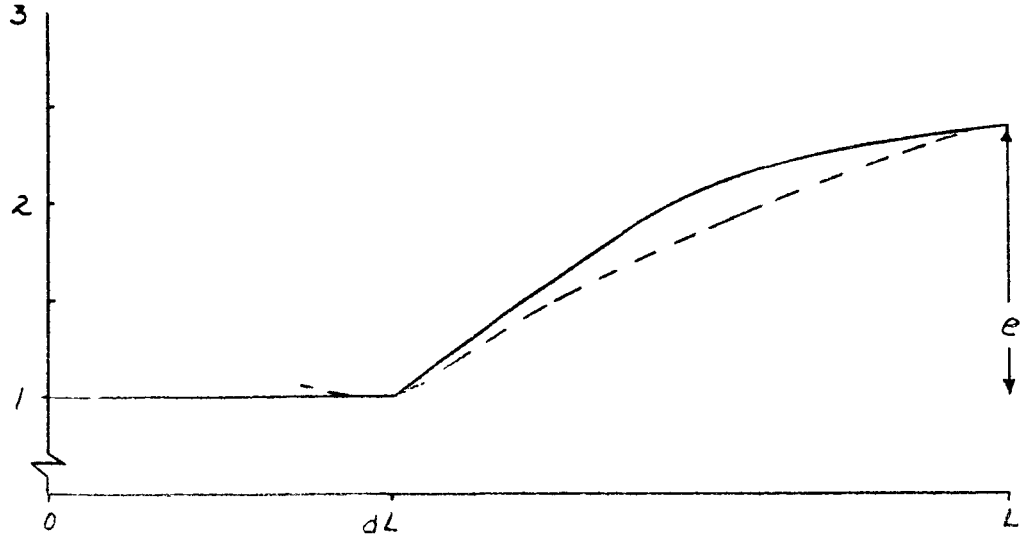

TABLE I

Centaur Interstage Adapter Data

590 lb. adapter

$\rho h = 4.46 \times 10^{-2}$ slugs/ft^2

$\Phi_o = 0.302$ (lb/ft^2)^2 /cps

$EI_s = 1.01 \times 10^4$ lb ft^2

$EI_\chi = 1.93 \times 10^3$ lb ft^2

1539 lb. adapter

$\rho h = 1.16 \times 10^{-1}$ slugs/ft^2

$\Phi_o = 0.302$ (lb/ft^2)^2 /cps

$EI_s = 4.55 \times 10^4$ lb ft^2

$EI_\chi = 1.93 \times 10^3$ lb ft^2

NATURAL FREQUENCIES AND DAMPING RATIOS

	*		**
	ω rad/sec	ζ	ω rad
ω_{12}	423	$\zeta_{12} = 0.01$ †	366
ω_{13}	314	$\zeta_{13} = 0.007$	334
ω_{14}	368	$\zeta_{14} = 0.012$	485
ω_{15}	477	$\zeta_{15} = 0.0035$	755
ω_{16}	553	$\zeta_{16} = 0.01$	1080
ω_{17}	766	$\zeta_{17} = 0.01$	1480
ω_{33}	880	$\zeta_{33} = 0.01$	691
ω_{34}	785	$\zeta_{34} = 0.01$	755
ω_{35}	628	$\zeta_{35} = 0.01$	866
ω_{36}	680	$\zeta_{36} = 0.01$	1136

* Fort Worth Vibration Test

** Computed Values from Reference 5.

*** Fort Worth DAMAC Analysis

† Estimated Damping

ζ_{ij} are the same

TABLE I (Continued)

AMPLITUDE COEFFICIENTS

$C_{12} = 0.891$
$C_{13} = 0.943$
$C_{14} = 0.967$
$C_{15} = 0.979$
$C_{16} = 0.985$
$C_{17} = 0.989$

$C_{33} = 0.974$
$C_{34} = 0.976$
$C_{35} = 0.981$
$C_{36} = 0.985$

FORCE DISTRIBUTION CONSTANTS (cf. EQUATION 2.16 AND FIGURE III)

INSULATION PANEL AND H_2 BOOST PUMP FAIRINGS

$A = 2.76$
$b = 0.3$
$c = 1.51$
$d = 0.355$
$e = 1.38$
$\Delta S = 2.0$ ft

6 OTHER FAIRINGS

$D = 2.74$
$\Delta S = 0.5$ ft
$S_1 = 19.8$ ft
$S_2 = 23.6$ ft
$S_3 = 27.7$ ft
$S_4 = 4.1$ ft
$S_5 = 7.7$ ft
$S_6 = 12.0$ ft

TABLE II

Cylindrical Shell Natural Frequencies for the 590 lb Adapter

m \ n	0	1	2	3	4	5	6	7	8	9	10
1	3892	2403	1235	687	434	329	318	368	455	565	693
2	5216	4225	2902	1957	1355	984	766	658	637	682	772
3	5248	4813	3909	3017	2304	1779	1410	1164	1019	960	973
4	5259	5020	4433	3728	3065	2506	2065	1734	1500	1354	1287
5	5267	5116	4717	4183	3622	3100	2650	2282	1997	1793	1665
6	5275	5172	4887	4481	4021	3563	3139	2772	2468	2232	2064
7	5287	5212	5000	4686	4313	3921	3541	3194	2893	2647	2459
8	5304	5247	5085	4837	4534	4203	3870	3554	3271	3029	2835
9	5327	5283	5155	4958	4710	4432	4144	3864	3604	3377	3188
10	5359	5324	5222	5062	4858	4626	4380	4135	3903	3695	3518

$a = 5.0$ ft.

$L = 13.106$ ft.

$h = 2.15 \times 10^{-2}$ ft.

$\rho = 2.075$ slugs/ft^3

$\nu = 0.316$

$E = 1.44 \times 10^{9}$ lb/ft^2

m = axial mode number

n = circumferential mode number

Frequencies are given in $\frac{\text{rad}}{\text{sec}}$.

TABLE III

RMS Results at the Antinodes ($x = \frac{L}{2}$, $s = 0$) for Various Adapter Configurations

	Hand Calculations			Digital Computer Results		
	590	590 + 422	1539	590	590 + 422	1539
W_{RMS} (in)	0.338	0.296	0.105	0.225 (18%)*	0.197	0.069 (13%)
$M_{X_{RMS}}$ (in lb)	121.0	106.0	40.4	845.0 (75%)	739.0	252.0 (70%)
$M_{S_{RMS}}$ (in lb)	2650.0	2320.0	2620.0	5700.0 (-1%)	4980.0	6170.0 (-10%)
$Q_{S_{RMS}}$ (lb)	234.0	204.0	203.0	N.A.	N.A.	N.A.

* Indicates contribution of the quadruple summation term in Equation 1.26 to the total mean square value.

TABLE IV

Modal Contributions to the Mean Square Bending Moment in the Rings

590 lb Adapter		% of Total	1539 lb Adapter		% of Total
H_{12}	$= 0.118 \times 10^{-7}$	0.37	H_{12}	$= 0.183 \times 10^{-7}$	1.80
H_{13}	$= 2.32 \times 10^{-7}$	7.33	H_{13}	$= 1.93 \times 10^{-7}$	19.00
H_{14}	$= 4.18 \times 10^{-7}$	13.20	H_{14}	$= 1.83 \times 10^{-7}$	18.00
H_{15}	$= 10.30 \times 10^{-7}$	32.50	H_{15}	$= 2.58 \times 10^{-7}$	25.40
H_{16}	$= 4.83 \times 10^{-7}$	15.30	H_{16}	$= .654 \times 10^{-7}$	6.40
H_{17}	$= 3.58 \times 10^{-7}$	11.30	H_{17}	$= .512 \times 10^{-7}$	5.00
H_{33}	$= .108 \times 10^{-7}$	0.34	H_{33}	$= .222 \times 10^{-7}$	2.10
H_{34}	$= .652 \times 10^{-7}$	2.06	H_{34}	$= .739 \times 10^{-7}$	7.20
H_{35}	$= 2.06 \times 10^{-7}$	6.50	H_{35}	$= .790 \times 10^{-7}$	7.80
H_{36}	$= 3.50 \times 10^{-7}$	11.10	H_{36}	$= .750 \times 10^{-7}$	7.30
Total	31.65×10^{-7}	100%	Total	10.17×10^{-7}	100%

LIST OF SYMBOLS

a	- mean radius of cylindrical shell
A, D_k	- circumferential force amplitudes
A_{ij}, B_{ij}, C_{ij}	- amplitude coefficients
b, d	- defined in Figure III
c, e	- sine wave amplitudes
D_{ijk}	- defined in Equation 1.24
E	- Youngs modulus
$F(x,y,z,t)$	- system forcing function
$h_{ij}(t)$	- impulse response function
$H_{ij}(i\omega)$	- complex frequency response function
h	- thickness of cylindrical shell
I_x, I_s	- area moment of inertia of stringers and rings
$K_{ijk}(i\omega)$	- defined in Equation 1.21
L	- length of cylindrical shell
M_x, M_s	- stringer and ring bending moments
M_{ij}	- generalized mass bending moments
$P(x,y,z)$	- defined in Equation 1.4
P_{ij}	- defined in Equation 1.5
Q_s	- shear in rings
$Q_{ij}(t)$	- generalized force
$q_{ij}(t)$	- generalized coordinates
$R_f(\tau)$	- autocorrelation function
ΔS, ΔS_k	- half arc length of protuberances
u, v, w	- longitudinal, circumferential, and radial displacements

$\alpha(x, y, z, t)$	- response function
$\alpha_{ij}(x, y, z)$	- spatial response function of $ij^{\underline{th}}$ mode
ξ_{ij}, ξ	- damping of the $ij^{\underline{th}}$ mode
ρ	- material density of cylindrical shell
ρh	- mass/unit area of adapter
$\phi_{ij}, \alpha_{ij}, \beta_{ij}, \gamma_{ij},$	- normal modes
$\Phi_f(\omega)$	- power spectral density function
Φ_o	- white noise power spectral density
ω_{ij}	- natural frequency of $ij^{\underline{th}}$ mode

REFERENCES

1. Fontenot, L. L., Response of Linear Mechanical Systems to Random Excitation, unpublished notes.

2. Mitchell, R. R., Supersonic Flutter of a Cylindrical Shell with Application to the Centaur Interstage Adapter, General Dynamics/Astronautics Report AY62-0069, January 1963.

3. Keating, M. P., Normal Mode Investigation of the Centaur Interstage Adapter, General Dynamics/ Fort Worth Report FZM-55-003, December 1961

4. Serrani, T., Buffeting Pressures for Centaur AC-2 Adapter General Dynamics/Astronautics Memorandum SD-63-207-AWS.

5. Tersteeg, G., Frequency Analysis of Stiffened Cylindrical Shells with Simply Supported Edges, General Dynamics/Astronautics Report 63-1067, to be published.